

# Banded Gas and Nongray Surface Radiation Models for High-Emissivity Coatings

Geraldine J. Heynderickx

Laboratory for Petrochemical Engineering, Ghent University, Krijgslaan 281, B9000 Ghent, Belgium

Masatsugu Nozawa

Asahi Kasei Co., Base Petrochemicals Production Dept. 3-13, Ushio-dori, Kurashiki, 712-8633 Okayama, Japan

DOI 10.1002/aic.10514

Published online July 18, 2005 in Wiley InterScience (www.interscience.wiley.com).

*The efficiency of the application of high-emissivity coatings on reactor tubes and furnace walls in steam-cracking technology can be evaluated only on the basis of a description of radiative heat transfer in frequency bands. For the flue gases in the furnace, a radiation model is introduced in which the gas emits and absorbs radiation in discrete bands only; for the surfaces a nongray surface approach is applied. First, the influence of the model changes on the calculated radiative energy exchange is evaluated theoretically. Next, different furnace simulations are performed to do a numerical evaluation of the introduction of banded radiation models. The changes in the furnace thermal efficiency, attributed to the application of high-emissivity coatings on furnace walls and tube skins in steam-cracking furnaces, are calculated. © 2005 American Institute of Chemical Engineers AIChE J, 51: 2721–2736, 2005*

**Keywords:** heat transfer, radiation, mathematical modeling, optimization, thermal cracking, high-emissivity coatings

## Introduction

Steam cracking of hydrocarbons to olefins is an endothermal process carried out in tubular reactor coils suspended in large gas-fired furnaces. Over 90% of the heat transfer from the furnace to the process gas in the reactor coils arises from radiation. An increase in the thermal efficiency of a furnace can be translated into an increase of yields, an increase of throughput, or a decrease in fuel gas input. Applying high-emissivity coatings in furnaces is believed to improve the heat transfer from furnace to reactor coils.<sup>1</sup> Coupled simulations of furnace and reactor coils are used to investigate the influence on the furnace thermal efficiency of such coatings. Obtaining reliable results for the radiative heat transfer in furnaces—absorption and (re-)emission of radiation by flue gas and surfaces, and reflection of radiation by surfaces—requires that the radiative

heat transfer in the furnace is correctly described. Until now, a nonbanded gas radiation model and a gray surface radiation model have been used to calculate the radiative heat transfer and the temperature profiles in a steam-cracking furnace. However, these models are not capable of evaluating the effect of applying high-emissivity coatings on furnace walls and/or reactor tubes on the thermal efficiency of the furnace.<sup>2</sup> Therefore, the gas radiation model, in which the gray gas emits radiation over the entire frequency spectrum (further called the nonbanded gas radiation model) is replaced by a more realistic gas radiation model in which the gray gas emits and absorbs radiation in discrete bands only (further called the banded gas radiation model). The gray surface radiation model, in which the emissivity of the surface is considered to be wavelength independent, is replaced by a nongray surface radiation model, in which the emissivity of the wall becomes wavelength dependent. This is necessary for a correct evaluation of the effects of applying a high-emissivity coating on the furnace walls and/or the reactor tubes. This paper presents simulation results for a naphtha cracker with a staggered tube row configuration.

Correspondence concerning this article should be addressed to G. J. Heynderickx at geraldine.heynderickx@UGent.be.

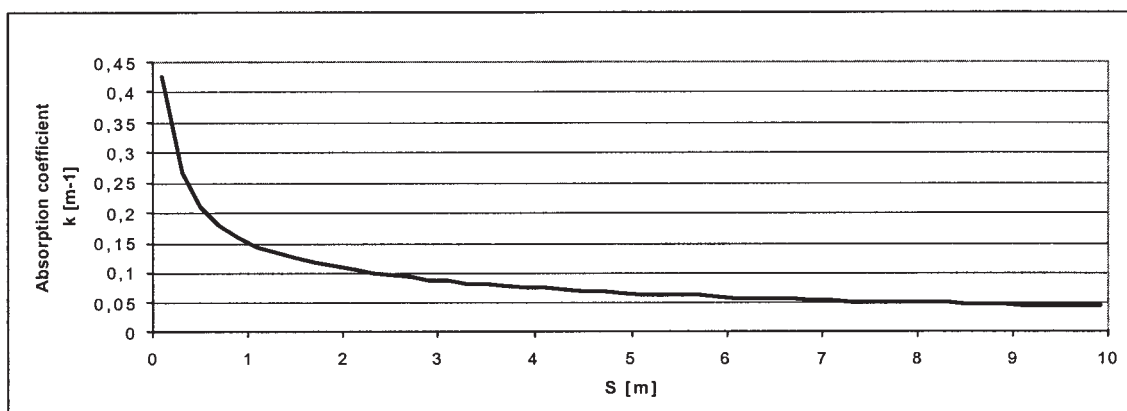


Figure 1. Absorption coefficient  $k$  as a function of the distance  $S$ .

$T_g = 1718.363$  K;  $p_{\text{CO}_2} = 8193.55$  Pa;  $p_{\text{H}_2\text{O}} = 17,253.4$  Pa;  $p_{\text{N}_2} = 72,344.5$  Pa ( $T_g$ , average temperature of the gas over distance  $S$ ).

## Radiation

The nature of radiative heat transfer is completely different from that of heat transfer by convection or conduction. Radiation is emitted by every body and is transported as an electromagnetic wave. No heat-exchanging medium is required.

When radiation hits a body, a fraction  $\alpha$  is absorbed by the body, a fraction  $\tau$  is transmitted through the body, and a fraction  $\rho$  is reflected by the body. For gases, reflection is negligible and absorption is small. For the solid materials typically used in radiation furnaces, transmission is zero and absorption is large. For the basic laws of radiative heat transfer, reference is made to any basic handbook of heat transfer.

A body or surface is called *gray* when its emissivity is wavelength independent. Its total hemispherical emissive power is then calculated according to

$$W = \epsilon(T)W_z = \epsilon(T)\sigma T^4 \quad (1)$$

Radiation in gases is fundamentally different from radiation by bodies/surfaces. Gases absorb and emit radiation at certain discrete frequencies, depending on the gas composition. In practice, these absorption lines turn into absorption bands. To overcome the difficulty of describing the phenomena of limited absorption in bands, the equivalent band concept is introduced: an absorption band is replaced by an equivalent absorption band in which absorption is complete and in which the same amount of energy is absorbed as in the original band. To determine the width of the equivalent band, the absorption model of Edwards<sup>3</sup> is used.<sup>4</sup> Carbon dioxide and water are the absorbing and emitting components in flue gases. The absorptivity of the flue gas is obtained by summing up the absorptivities of these absorbing components, correcting for possible overlap of the equivalent bands. From this value, the absorption coefficient  $k$  of the gas is calculated:

$$1 - \alpha(T) = 1 - \epsilon(T) = \exp(-kS) \quad (2)$$

The absorption coefficient strongly depends on the value of  $S$ , the distance traveled through the gas. The relation for a typical flue gas composition is presented in Figure 1. When the ab-

sorption coefficient is wavelength independent, the gas is called *gray*.

## Difficulties with nonbanded radiation approach to describe coating effects

To increase the thermal efficiency of a furnace, the use of high-emissivity coatings on reactor tubes and/or furnace walls has been suggested.<sup>1</sup> Applying a high-emissivity coating on a *reactor tube* decreases the amount of reflected energy and increases the amount of absorbed (and possibly reradiated) energy. Thus, the capacity of the reactor tube to transfer heat from the furnace to the process gas (that is, the gas inside the reactor tube) increases. Applying a high-emissivity coating on a *furnace wall* increases the amount of energy absorbed by the furnace wall. Because heat losses to the surroundings are small, more energy will be reradiated into the furnace. On the other hand, reflection of radiative energy on the furnace wall decreases accordingly. As a result, more energy will be transferred from the flue gas to the reactor tubes by the furnace wall after absorption and reradiation, at the cost of the amount of energy transferred from the flue gas to the reactor tubes by reflection on the furnace walls. Both reflection and emission of radiative energy by the furnace wall are diffuse. However, the fraction of the gas radiation that is *reflected* by the furnace walls preserves its spectral character. Its frequencies remain those of the absorption/emission bands of the gas. The fraction of the gas radiation that is *absorbed and reradiated* by the furnace walls is spread over the complete frequency spectrum because the furnace wall is a solid material. As a consequence, only part of the absorbed radiation is reradiated within the range of the absorption bands of the gas; the remaining part is reradiated in a so-called clear window,<sup>5-9</sup> and reaches the reactor tubes without possibly being absorbed by the gas.

Heat transfer could thus be more efficient by the application of high-emissivity coatings on the furnace walls and/or reactor tubes. It will be shown that, if a nonbanded gas radiation model is applied, that is, if the gas is considered to emit radiative energy over the entire wavelength spectrum, the effect of applying coatings on the thermal efficiency of the furnace cannot be evaluated. It is necessary to take into account that the

**Table 1. Data on Eight Absorption Bands and Nine Clear Windows\***

Band	Division ( $\mu\text{m}$ )	Type	Furnace Wall		Tube		Coating	
			G	NG	G	NG	G	NG
1	18.0<	No absorption band	0.59	0.85	0.85	0.28	0.95	0.95
2	12.0–18.0	CO <sub>2</sub> absorption band	0.59	0.85	0.85	0.28	0.95	0.95
3	10.6–12.0	No absorption band	0.59	0.85	0.85	0.3	0.95	0.95
4	10.2–10.6	CO <sub>2</sub> absorption band	0.59	0.85	0.85	0.32	0.95	0.95
5	9.6–10.2	No absorption band	0.59	0.85	0.85	0.4	0.95	0.95
6	9.2–9.6	CO <sub>2</sub> absorption band	0.59	0.85	0.85	0.34	0.95	0.95
7	9.0–9.2	No absorption band	0.59	0.85	0.85	0.34	0.95	0.95
8	5.0–9.0	H <sub>2</sub> O absorption band	0.59	0.8	0.85	0.38	0.95	0.92
9	4.8–5.0	No absorption band	0.59	0.5	0.85	0.4	0.95	0.85
10	4.0–4.8	CO <sub>2</sub> absorption band	0.59	0.36	0.85	0.42	0.95	0.77
11	2.9–4.0	No absorption band	0.59	0.3	0.85	0.45	0.95	0.68
12	2.3–2.9	CO <sub>2</sub> , H <sub>2</sub> O absorption band	0.59	0.2	0.85	0.5	0.95	0.65
13	2.0–2.3	No absorption band	0.59	0.13	0.85	0.58	0.95	0.62
14	1.7–2.0	H <sub>2</sub> O absorption band	0.59	0.13	0.85	0.62	0.95	0.62
15	1.5–1.7	No absorption band	0.59	0.15	0.85	0.68	0.95	0.62
16	1.2–1.5	H <sub>2</sub> O absorption band	0.59	0.15	0.85	0.7	0.95	0.62
17	<1.2	No absorption band	0.59	0.13	0.85	0.74	0.95	0.62
		Gray emissivity (see Eq. 57)	0.59	0.386	0.85	0.451	0.95	0.738

\*Emissivity values given as a function of wavelength.<sup>10,11</sup> G, gray; NG, nongray.

gas radiates in separate wavelength bands. In the banded gas radiation model for flue gases, applied in this work, 17 bands are considered (see Table 1). It will also be shown that, if a gray surface radiation model is applied—that is, if the surface emissivity is considered constant over the entire wavelength spectrum—the effect of applying coatings on the thermal efficiency of the furnace cannot be evaluated. In reality, most solid materials behave as nongray materials; their emissivity has a wavelength-dependent value.<sup>10,11</sup> Different emissivity values for the different solid materials in the furnace and for the 17 wavelength bands, considered in this work, will be used during the calculations (see Table 1).

The influence of the introduction of the banded behavior of gas radiation and the nongray behavior of solids radiation on the calculated furnace performance will be evaluated theoretically in a first step. In a second step the theory will be supported by a number of calculation results.

## Model Equations and Simulation Procedure

A detailed description of the reactor model is given by Heynderickx and Froment.<sup>12</sup>

For the calculation of the actual heat transfer by radiation, the furnace model uses the zone method of Hottel and Sarofim,<sup>13</sup> further developed by Vercammen and Froment.<sup>14,15</sup> The furnace walls, the tubes, and the flue gas volume are divided into a number of surface and volume zones that are considered to be isothermal elements with constant properties. For each of these zones the energy balance is constructed taking into account conductive, convective, and radiative heat transfer. The contributions of radiative heat transfer are obtained through Monte Carlo simulation,<sup>16</sup> calculating the view factors  $F_{ij}^0$  between the isothermal elements in a transparent medium. From these view factors, the direct exchange areas between the zones are calculated, taking into account the absorption of energy between the zones in a nontransparent medium (the flue gas). A direct exchange area  $z_i z_j$  is a measure for the amount of radiative energy emitted by a zone  $i$  and absorbed by a zone  $j$ , without considering reflection of energy.

From the direct exchange areas, the total exchange areas between the zones are calculated. The total exchange area  $Z_i Z_j$  is defined as the amount of radiative energy emitted by the zone  $i$  and finally absorbed by zone  $j$ , directly or after reflection, divided by  $W_{zi}$ , which is the total hemispherical emissivity of a black body with the same temperature as the emitter zone  $i$ . Determination of the total exchange areas from the direct exchange areas is discussed in detail by Rao et al.<sup>17</sup> and by Plehiers and Froment.<sup>16</sup> The set of energy balances in the furnace can be written as

$$\begin{pmatrix} Z_1 Z_1 - \sum_j Z_1 Z_j & Z_2 Z_1 & \cdots & Z_n Z_1 \\ Z_1 Z_2 & Z_2 Z_2 - \sum_j Z_2 Z_j & \cdots & Z_n Z_2 \\ \cdots & \cdots & \cdots & \cdots \\ Z_1 Z_n & Z_2 Z_n & \cdots & Z_n Z_n - \sum_j Z_n Z_j \end{pmatrix} \times \begin{pmatrix} W_{z1} \\ W_{z2} \\ \cdots \\ W_{zn} \end{pmatrix} = \begin{pmatrix} Q_1 A_1 \\ Q_2 A_2 \\ \cdots \\ Q_n A_n \end{pmatrix} \quad (3)$$

where  $Q_i$  represents the nonradiative heat flux emitted by zone  $i$ . This nonradiative heat flux considers convective, conductive, and/or flow contributions, depending on the nature of zone  $i$  (furnace wall, tube skin, flue gas volume). Solving this set of balances yields the heat flux and temperature profiles in the furnace. Replacing the nonbanded gas/gray surface radiation models by banded gas/nongray surface radiation models will affect the total exchange area calculation, and thus the calculated profiles, as described below.

## Calculation of the Total Exchange Areas with Banded Radiation Models

The effect of the introduction of models with varying radiation properties in different wavelength bands is illustrated by its influence on the calculated total exchange area values. First, the effect of the introduction of a banded gas radiation model to replace the nonbanded gas radiation model in an environment of gray surfaces is illustrated. Next, the effect of the introduction of a nongray surface radiation model is illustrated.

### General considerations

In a calculation with the nonbanded gas radiation model, one absorption/emission coefficient for each flue gas zone is calculated, and the emitted energy is distributed over the entire wavelength spectrum. In a calculation with the banded gas radiation model, one absorption/emission coefficient for each flue gas zone is calculated, but the emitted energy is distributed over eight frequency bands. In between these bands the so-called clear windows are found (Table 1). When replacing the gray surface radiation model with a constant emissivity value over the entire frequency spectrum, by the nongray surface radiation model, 17 emissivity values are defined for each surface material—one for each of the 17 bands used in the banded gas radiation model (Table 1).

In general, the total amount of radiation emitted by a body  $J$  is calculated from its total emissive power  $W$ , and the part of the radiation that reaches the body  $G$  and that is reflected by it:

$$J = W + \rho G = \varepsilon W_z + \rho G \quad (4)$$

Each of these values has a directional and a spectral dependency.

When the emitter is a surface zone, the total emission of the surface zone  $i$  in the spectral band  $b$  is calculated from<sup>16,17</sup>

$$A_i J_{i,b} = A_i \varepsilon_{i,b} W_{z,i,b} + \rho_{i,b} \left[ \sum_j^m s_j s_{i,b} J_{j(tot)} + \sum_k^n g_k s_{i,b} W_{z,gk(tot)} \right] \quad (5)$$

The directional distribution of the emitted energy is introduced by the direct exchange areas  $s_j s_i$  and  $g_k s_i$ , which are calculated by using a Monte Carlo simulation technique in which the Lambert law is considered to be valid. The spectral distribution of the emitted energy is taken into account by the introduction of the band-dependent emissivity  $\varepsilon_{i,b}$  and the band-dependent reflectivity  $\rho_{i,b}$  of the surface material. If the surface is considered to be a gray surface, these values are band independent. The direct exchange area from surface zone  $j$  to surface zone  $i$  in a band  $b$ ,  $s_j s_{i,b}$ , is obtained by multiplying the view factor between those zones with the area of the emitting surface

$$s_j s_{i,b} = F_{ji}^0 A_j f_b \tau_{ji,b} \quad (6)$$

taking into account that only a fraction  $f_b$  of the radiation is emitted in band  $b$ , and taking into account a possible absorption of radiation in band  $b$  by the gas between both zones.

“Direct” refers to the fact that no reflected energy is consid-

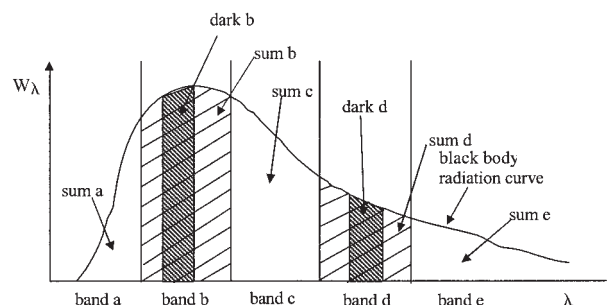


Figure 2. Five-band sample calculation image for direct exchange area calculation in bands.

ered. The view factor is calculated by a Monte Carlo simulation. Its value is determined by the geometry of the furnace and the isothermal zones that are defined in the furnace.

The direct exchange area from a gas zone  $k$  to a surface zone  $i$ ,  $g_k s_{i,b}$ , is obtained from

$$g_k s_{i,b} = 4k_k V_k F_{ki}^0 f_b \tau_{ki,b} \quad (7)$$

The direct exchange areas over the entire wavelength spectrum are obtained by summing up the contributions in all emission bands.

### Direct exchange area calculation with a nonbanded and a banded gas radiation model in an environment of gray surfaces

In the nonbanded gas radiation model, one direct exchange area between two zones is calculated based on the view factor value and on the transmissivity value that is calculated with the equivalent band concept.<sup>16</sup> In the banded gas radiation model, a direct exchange area between two zones is calculated in each of the 17 bands, based on the view factor value, on the fraction of energy emitted in the considered band and on 17 transmissivity values—one for each of the 17 bands. In the banded gas radiation model, no radiation is emitted or absorbed by the gas in the so-called clear windows: the transmissivity for radiative energy emitted by a surface in a clear window is one. In the absorption bands, the transmissivity for radiative energy (emitted by a gas or a surface) is calculated from the equivalent band concept. The different results obtained with the nonbanded and the banded gas radiation approach are illustrated by means of a sample calculation.

A sample calculation, in which the wavelength spectrum is divided in five bands, is performed starting from Figure 2. The black body emissive power of the emitting gas zone  $k$ ,  $W_{zk}$ , is given a value of one in the sample calculation.

When using the nonbanded gas radiation model, the black body radiative energy of the gas is emitted over the entire wavelength spectrum

$$\text{sum a} + \text{sum b} + \text{sum c} + \text{sum d} + \text{sum e} = 1 \quad (8)$$

Sum  $b$  is the total area in band  $b$ . In Figure 2, *dark b* is the shaded area calculated from the equivalent band absorption model of Edwards,<sup>3</sup> as discussed above. Because only in bands  $b$  and  $d$  is radiative energy absorbed,

$$dark\ a = dark\ c = dark\ e = 0 \quad (9)$$

according to the equivalent band concept.

When the gas is considered to be a nonbanded gray gas, emitting over the entire wavelength spectrum, the direct exchange area from, say, an emitting gas zone  $k$  to an absorbing surface zone  $i$ , in the different bands is calculated from (see Eq. 7)

$$g_k S_{i_a} = 4k_k V_k F_{ki}^0 * \frac{\sum_{z=a}^e \sum z}{\sum z} * \left[ 1 - \frac{dark\ a}{\sum a} \right] = 4k_k V_k F_{ki}^0 * f_a \quad (10)$$

$$g_k S_{i_b} = 4k_k V_k F_{ki}^0 * \frac{\sum_{z=a}^e \sum z}{\sum z} * \left[ 1 - \frac{dark\ b}{\sum b} \right] = 4k_k V_k F_{ki}^0 * f_b * \tau_{ki_b} \quad (11)$$

$$g_k S_{i_c} = 4k_k V_k F_{ki}^0 * \frac{\sum_{z=a}^e \sum z}{\sum z} * \left[ 1 - \frac{dark\ c}{\sum c} \right] = 4k_k V_k F_{ki}^0 * f_c \quad (12)$$

$$g_k S_{i_d} = 4k_k V_k F_{ki}^0 * \frac{\sum_{z=a}^e \sum z}{\sum z} * \left[ 1 - \frac{dark\ d}{\sum d} \right] = 4k_k V_k F_{ki}^0 * f_d * \tau_{ki_d} \quad (13)$$

$$g_k S_{i_e} = 4k_k V_k F_{ki}^0 * \frac{\sum_{z=a}^e \sum z}{\sum z} * \left[ 1 - \frac{dark\ e}{\sum e} \right] = 4k_k V_k F_{ki}^0 * f_e \quad (14)$$

By adding up over all five bands of the sample calculation

$$g_k S_{i(\text{nonbanded gas, gray surface})} = 4k_k V_k F_{ki}^0 * [1 - (dark\ b + dark\ d)] = 4k_k V_k F_{ki}^0 * \tau_{ki(\text{nonbanded gas, gray surface})} \quad (15)$$

as

$$f_a + f_b + f_c + f_d + f_e = 1 \quad (16)$$

When the gas is considered to be a banded gray gas, emitting in bands  $b$  and  $d$  only, the direct exchange area from an emitting gas zone  $k$  to an absorbing surface zone  $i$  is calculated from

$$g_k S_{i_a} = 0 \quad (\text{clear window}; f_a = 0) \quad (17)$$

$$g_k S_{i_b} = 4k_k V_k F_{ki}^0 * \frac{dark\ b}{dark\ b + dark\ d} * \left( 1 - \frac{dark\ b}{\sum b} \right) = 4k_k V_k F_{ki}^0 * f_b * \tau_{ki_b} \quad (18)$$

$$g_k S_{i_c} = 0 \quad (\text{clear window}; f_c = 0) \quad (19)$$

$$g_k S_{i_d} = 4k_k V_k F_{ki}^0 * \frac{dark\ d}{dark\ b + dark\ d} * \left( 1 - \frac{dark\ d}{\sum d} \right) = 4k_k V_k F_{ki}^0 * f_d * \tau_{ki_d} \quad (20)$$

$$g_k S_{i_e} = 0 \quad (\text{clear window}; f_e = 0) \quad (21)$$

By adding up over all bands

$$g_k S_{i(\text{banded gas, gray surface})} = 4k_k V_k F_{ki}^0 * \left\{ 1 - \left[ \frac{dark\ b}{(dark\ b + dark\ d)} \frac{dark\ b}{\sum b} + \frac{dark\ d}{(dark\ b + dark\ d)} \frac{dark\ d}{\sum d} \right] \right\} = 4k_k V_k F_{ki}^0 * \tau_{ki(\text{banded gas, gray surface})} \quad (22)$$

as

$$f_b + f_d = 1 \quad (23)$$

and using Kirchoff's law by introducing

$$\frac{emission\ b}{emission\ b + emission\ d} = \frac{dark\ b}{dark\ b + dark\ d} \quad (24)$$

In the last equation, *emission b* stands for the amount of radiative energy emitted by the gas in band  $b$ :

$$emission\ b + emission\ d = 4k_k V_k W_{zk} = 4k_k V_k \quad (25)$$

Analogous derivations can be made for the direct exchange area calculation between two surface zones, between two gas zones or from a surface zone to a gas zone.

### Direct exchange area calculation with a banded gas radiation model in an environment of gray and nongray surfaces

When surface  $j$  is considered to be a gray surface, the emissivity  $\varepsilon_{j_b}$  in each of the 17 considered emission bands has a constant value. For a nongray surface the emissivity value differs in each of the 17 bands. A sample calculation is performed starting from Figure 2. The direct exchange area from the emitting surface zone  $j$  to an absorbing surface zone  $i$  in each of the bands is then calculated according to the following concepts. The black body emissive power of the emitting zone  $j$ ,  $W_{zj}$ , is given a value of one in the sample calculation.

When the surface zone is considered to be a gray surface, that is, with a constant emissivity, the direct exchange area from the emitting zone  $j$  to the receiving zone  $i$  is calculated from (see Eq. 6):



$$s_j s_{i_a} = F_{ji}^0 A_j * \frac{\varepsilon_j \text{sum } a}{\sum_{z=a}^e \varepsilon_j \text{sum } z} * \left(1 - \frac{\text{dark } a}{\text{sum } a}\right) = F_{ji}^0 A_j * f_a \quad (26)$$

$$s_j s_{i_b} = F_{ji}^0 A_j * \frac{\varepsilon_j \text{sum } b}{\sum_{z=a}^e \varepsilon_j \text{sum } z} * \left(1 - \frac{\text{dark } b}{\text{sum } b}\right) = F_{ji}^0 A_j * f_b * \tau_{ji_b} \quad (27)$$

$$s_j s_{i_c} = F_{ji}^0 A_j * \frac{\varepsilon_j \text{sum } c}{\sum_{z=a}^e \varepsilon_j \text{sum } z} * \left(1 - \frac{\text{dark } c}{\text{sum } c}\right) = F_{ji}^0 A_j * f_c \quad (28)$$

$$s_j s_{i_d} = F_{ji}^0 A_j * \frac{\varepsilon_j \text{sum } d}{\sum_{z=a}^e \varepsilon_j \text{sum } z} * \left(1 - \frac{\text{dark } d}{\text{sum } d}\right) = F_{ji}^0 A_j * f_d * \tau_{ji_d} \quad (29)$$

$$s_j s_{i_e} = F_{ji}^0 A_j * \frac{\varepsilon_j \text{sum } e}{\sum_{z=a}^e \varepsilon_j \text{sum } z} * \left(1 - \frac{\text{dark } e}{\text{sum } e}\right) = F_{ji}^0 A_j * f_e \quad (30)$$

taking into account Eq. 9.

By adding up over all five bands of the sample calculation,

$$s_j s_{i(\text{banded gas, gray surface})} = F_{ji}^0 A_j * [1 - (\text{dark } b + \text{dark } d)] = F_{ji}^0 A_j * \tau_{ji(\text{banded gas, gray surface})} \quad (31)$$

taking into account Eqs. 8 and 16.

When the surface zone is considered to be a nongray surface:

$$s_j s_{i_a} = F_{ji}^0 A_j * \frac{\varepsilon_{j_a} \text{sum } a}{\sum_{z=a}^e \varepsilon_{j_z} \text{sum } z} * \left(1 - \frac{\text{dark } a}{\text{sum } a}\right) = F_{ji}^0 A_j * f_a \quad (32)$$

$$s_j s_{i_b} = F_{ji}^0 A_j * \frac{\varepsilon_{j_b} \text{sum } b}{\sum_{z=a}^e \varepsilon_{j_z} \text{sum } z} * \left(1 - \frac{\text{dark } b}{\text{sum } b}\right) = F_{ji}^0 A_j * f_b * \tau_{ji_b} \quad (33)$$

$$s_j s_{i_c} = F_{ji}^0 A_j * \frac{\varepsilon_{j_c} \text{sum } c}{\sum_{z=a}^e \varepsilon_{j_z} \text{sum } z} * \left(1 - \frac{\text{dark } c}{\text{sum } c}\right) = F_{ji}^0 A_j * f_c \quad (34)$$

$$s_j s_{i_d} = F_{ji}^0 A_j * \frac{\varepsilon_{j_d} \text{sum } d}{\sum_{z=a}^e \varepsilon_{j_z} \text{sum } z} * \left(1 - \frac{\text{dark } d}{\text{sum } d}\right) = F_{ji}^0 A_j * f_d * \tau_{ji_d} \quad (35)$$

$$s_j s_{i_e} = F_{ji}^0 A_j * \frac{\varepsilon_{j_e} \text{sum } e}{\sum_{z=a}^e \varepsilon_{j_z} \text{sum } z} * \left(1 - \frac{\text{dark } e}{\text{sum } e}\right) = F_{ji}^0 A_j * f_e \quad (36)$$

By adding up over all bands, taking into account Eqs. 8 and 16,

$$s_j s_{i(\text{banded gas, nongray surface})} = F_{ji}^0 A_j * \left[1 - \left(\frac{\varepsilon_{j_b} \text{dark } b + \varepsilon_{j_d} \text{dark } d}{\sum_{z=a}^e \varepsilon_{j_z} \text{sum } z}\right)\right] = F_{ji}^0 A_j * \tau_{ji(\text{banded gas, nongray surface})} \quad (37)$$

Analogous derivations can be made for the other direct exchange areas.

From the above Eqs. 6 and 31 it is easily understood that the introduction of a banded gas radiation model in an environment of gray surfaces has no influence on the calculated direct exchange area between two surface zones when the equivalent band concept is used to calculate the absorption of radiation between the emitting and the absorbing zone in both the non-banded and the banded gas radiation model

$$s_j s_{i(\text{nonbanded gas, gray surface})} = \left(\sum_{b=1}^{17} s_j s_{i_b}\right)_{(\text{banded gas, gray surface})} \quad (38)$$

Equation 38 implies that the average gas temperature between the two zones, which also determines the transmissivity values, changes only slightly when the banded gas radiation model is introduced. On the contrary, the direct exchange area from a gas zone  $k$  to a surface zone  $i$  will be affected by the introduction of the banded gas radiation model in an environment of gray surfaces (reference is made to Eqs. 7, 15, and 22)

$$g_k s_{i(\text{nonbanded gas, gray surface})} \neq \left(\sum_{b=1}^{17} g_k s_{i_b}\right)_{(\text{banded gas, gray surface})} \quad (39)$$

because in the banded gas radiation model the energy emitted by the gas is divided over a limited number of bands, whereas for the nonbanded gas radiation model the entire wavelength spectrum is considered for energy radiation. The use of the equivalent band concept to calculate the absorption of radiation between the zones, in combination with the different gas radiation models, will give different results.

On the other hand, from Eq. 6 and the sample calculation (considering Eqs. 31 and 37), it is easily understood that the direct exchange area between two surfaces will be affected by replacing the gray surface radiation model by the nongray surface radiation model

$$\left( \sum_{b=1}^{17} S_j S_{i-b} \right)_{(\text{banded gas, gray surface})} \neq \left( \sum_{b=1}^{17} S_j S_{i-b} \right)_{(\text{banded gas, nongray surface})} \quad (40)$$

For both gray and nongray surfaces, the equivalent band absorption model is used to calculate the absorption of radiative energy between the two surface zones.

It can easily be proved by a comparable sample calculation that the direct exchange area from a gas zone  $k$  to a surface zone  $i$  will not be affected by the introduction of the nongray surface radiation model (if the transmissivity of the gas remains unchanged, that is, if the temperature of the gas in between the two zones remains unchanged)

$$\left( \sum_{b=1}^{17} g_k S_{i-b} \right)_{(\text{banded gas, gray surface})} = \left( \sum_{b=1}^{17} g_k S_{i-b} \right)_{(\text{banded gas, nongray surface})} \quad (41)$$

### Total exchange area calculation

The effect of the results discussed above on the total exchange area calculations can now be evaluated. Equation 5 is valid for each of the surface zones in the simulated environment. If the surface zone  $i$  is considered to be the only emitter in the system, with a total black body emissive power of 1, the set of Eq. 5 for all zones, considering band  $b$ , can be written in matrix form as

$$\begin{bmatrix} \frac{A_1}{\rho_{1-b}} & 0 & 0 & 0 & 0 \\ 0 & \frac{A_2}{\rho_{2-b}} & 0 & 0 & 0 \\ 0 & 0 & \cdots & 0 & 0 \\ 0 & 0 & 0 & \cdots & 0 \\ 0 & 0 & 0 & 0 & \frac{A_m}{\rho_{m-b}} \end{bmatrix} \begin{bmatrix} J_{1-b} \\ J_{2-b} \\ \vdots \\ J_{m-b} \end{bmatrix} = \begin{bmatrix} 0 \\ 0 \\ \frac{A_i \epsilon_{i-b}}{\rho_{i-b}} W_{z, Si-b} \\ 0 \\ 0 \end{bmatrix} + \begin{bmatrix} S_1 S_{1-b} & S_2 S_{1-b} & \cdots & S_m S_{1-b} \\ S_1 S_{2-b} & S_2 S_{2-b} & \cdots & S_m S_{2-b} \\ \vdots & \vdots & \ddots & \vdots \\ S_1 S_{m-b} & S_2 S_{m-b} & \cdots & S_m S_{m-b} \end{bmatrix} \begin{bmatrix} J_{1(tot)} \\ J_{2(tot)} \\ \vdots \\ J_{m(tot)} \end{bmatrix} \quad (42)$$

where  $W_{z, Si-b}$  is the fraction of energy radiated by the black body surface zone  $i$  in band  $b$ . Introducing the concept of total exchange area  $S_i S_{j-b}$ , defined as the energy emitted by surface zone  $i$  and finally absorbed by surface zone  $j$ , directly or after reflection, divided by the total hemispherical emissivity of a black body with the same temperature as the emitter, one obtains

$$J_{j-b} = \frac{S_i S_{j-b} \rho_{j-b}}{A_j \cdot \epsilon_{j-b}} + \delta_{ij} \epsilon_{j-b} W_{z, sj-b} \quad (43)$$

By introducing Eq. 43 into Eq. 42, the matrix formulation becomes

$$\begin{bmatrix} \frac{S_i S_{1-b}}{\epsilon_{1-b}} \\ \frac{S_i S_{2-b}}{\epsilon_{2-b}} \\ \vdots \\ \frac{S_i S_{m-b}}{\epsilon_{m-b}} \end{bmatrix} = \begin{bmatrix} S_1 S_{1-b} & S_2 S_{1-b} & \cdots & S_m S_{1-b} \\ S_1 S_{2-b} & S_2 S_{2-b} & \cdots & S_m S_{2-b} \\ \vdots & \vdots & \ddots & \vdots \\ S_1 S_{m-b} & S_2 S_{m-b} & \cdots & S_m S_{m-b} \end{bmatrix} \begin{bmatrix} J_{1(tot)} \\ J_{2(tot)} \\ \vdots \\ J_{m(tot)} \end{bmatrix} \quad (44)$$

When the surfaces are considered to be gray surfaces, emissivity and reflectivity values in the above equations become band independent.

By adding up over all 17 bands in an environment of gray surfaces, and taking into account Eq. 38, it is easily understood that the introduction of the banded gas radiation model to replace the nonbanded gas radiation model does not influence the total exchange area between two surface zones

$$S_i S_{j(\text{nongray gas, gray surface})} = \left( \sum_{b=1}^{17} S_i S_{j-b} \right)_{(\text{banded gas, gray surface})} \quad (45)$$

On the other hand, by adding up over all 17 bands, and taking into account Eq. 40, it is easily understood that the introduction of the nongray surface radiation model to replace the gray surface radiation model does influence the total exchange area between two surface zones

$$\left( \frac{1}{\epsilon_j} \sum_{b=1}^{17} S_i S_{j-b} \right)_{(\text{banded gas, gray surface})} \neq \left( \sum_{b=1}^{17} \frac{S_i S_{j-b}}{\epsilon_{j-b}} \right)_{(\text{banded gas, nongray surface})} \quad (46)$$

or

$$\left( \sum_{b=1}^{17} S_i S_{j-b} \right)_{(\text{banded gas, gray surface})} \neq \left( \sum_{b=1}^{17} S_i S_{j-b} \right)_{(\text{banded gas, nongray surface})} \quad (47)$$

It must be remarked that the total emission  $J_{i(tot)}$  of a zone depends on total exchange area values. However, as the calculation of a furnace proceeds iteratively, total emission values of a previous iteration step can be used during the calculations.

If analogous developments are made for a system where a gas zone  $k$  is considered to be the only emitter, one obtains

$$J_{j-b} = \frac{G_k S_{j-b} \rho_{j-b}}{A_j \epsilon_{j-b}} \quad (48)$$

The corresponding matrix formulation becomes

$$\begin{bmatrix} \frac{G_k S_{1-b}}{\epsilon_{1-b}} \\ \frac{G_k S_{2-b}}{\epsilon_{2-b}} \\ \vdots \\ \frac{G_k S_{m-b}}{\epsilon_{m-b}} \end{bmatrix} = \begin{bmatrix} S_{1S_{1-b}} & S_{2S_{1-b}} & \cdots & S_{mS_{1-b}} \\ S_{1S_{2-b}} & S_{2S_{2-b}} & \cdots & S_{mS_{2-b}} \\ \vdots & \vdots & \ddots & \vdots \\ S_{1S_{m-b}} & S_{2S_{m-b}} & \cdots & S_{mS_{m-b}} \end{bmatrix} \begin{bmatrix} J_{1(tot)} \\ J_{2(tot)} \\ \vdots \\ J_{m(tot)} \end{bmatrix} + \begin{bmatrix} g_k S_{1-b} \\ g_k S_{2-b} \\ \vdots \\ g_k S_{m-b} \end{bmatrix} \quad (49)$$

From Eqs. 39 and 49 it is clear that the introduction of the banded gas radiation model to replace the nonbanded gas radiation model in an environment of gray surfaces influences the total exchange area from a gas zone to a surface zone:

$$G_k S_{i(\text{nonbanded gas, gray surface})} \neq \left( \sum_{b=1}^{17} G_k S_{i-b} \right)_{(\text{banded gas, gray surface})} \quad (50)$$

From Eqs. 40, 41, and 49 it follows that the introduction of the nongray surface radiation model to replace the gray surface radiation model affects the total exchange area from a gas zone to a surface zone:

$$\left( \sum_{b=1}^{17} G_k S_{i-b} \right)_{(\text{banded gas, gray surface})} \neq \left( \sum_{b=1}^{17} G_k S_{i-b} \right)_{(\text{banded gas, nongray surface})} \quad (51)$$

Comparable considerations can be made when the emitting zone is a surface zone and the absorbing zone is a gas zone, resulting in

$$S_j G_{k(\text{nonbanded gas, gray surface})} = \left( \sum_{b=1}^{17} S_j G_{k-b} \right)_{(\text{banded gas, gray surface})} \quad (52)$$

and

$$\left( \sum_{b=1}^{17} S_j G_{k-b} \right)_{(\text{banded gas, gray surface})} \neq \left( \sum_{b=1}^{17} S_j G_{k-b} \right)_{(\text{banded gas, nongray surface})} \quad (53)$$

For the exchange between two gas zones, one obtains

$$G_k G_{i(\text{nonbanded gas, gray surface})} \neq \left( \sum_{b=1}^{17} G_k G_{i-b} \right)_{(\text{banded gas, gray surface})} \quad (54)$$

and

$$\left( \sum_{b=1}^{17} G_k G_{i-b} \right)_{(\text{banded gas, gray surface})} \neq \left( \sum_{b=1}^{17} G_k G_{i-b} \right)_{(\text{banded gas, nongray surface})} \quad (55)$$

From the above approach, it is clear that the introduction of the banded gas radiation model to replace the nonbanded gas radiation model in a furnace environment where the surfaces are considered to be gray surfaces, the total exchange area between two zones, as a measure for radiative heat exchange between these zones, remains unchanged if the radiation emitting zone is a surface zone (Eqs. 45 and 52), whereas the total exchange area between two zones changes if the radiation emitting zone is a gas zone (Eqs. 50 and 54).

From the above approach, it is also clear that by the introduction of the nongray surface radiation model to replace the gray surface radiation model in a furnace environment, all total exchange areas—as a measure for radiative heat exchange—change, regardless of the fact that the energy emitting zone is a surface zone (Eqs. 47 and 53) or a gas zone (Eqs. 51 and 55). As a new modeling approach is introduced for the surface, the direct exchange areas between surface zones become affected (see Eq. 40), and therefore all total exchange areas change.

The practical impact of the introduction of the banded gas and nongray surface radiation model on the furnace calculation results will be discussed below, presenting calculation results for both a noncoated furnace and a coated furnace. However, before doing so, special attention is given to the calculation of the radiative energy emitted by a gas zone  $k$ ,  $4k_k V_k W_{zk}$ .

### Emissive beam length calculation

When the nonbanded gas radiation model is used, one single value of the emissive beam length is calculated for the entire furnace. This emissive beam length, based on the volume and the furnace wall surface area of the complete furnace

$$S_{(\text{nonbanded gas})}^{(e)} = \frac{4V}{A} \quad (56)$$

is used to calculate the absorption coefficient for each gas zone in the furnace (Eq. 2). With this simplified approach good results are obtained when comparing the calculated furnace thermal efficiency to the industrial value ( $\pm 45\%$ ). If this simplified approach for the emissive beam length calculation is used in combination with the banded gas radiation model, the calculated thermal efficiency of the furnace decreases by more than 5%. This is attributed to an increase of the (self-)absorption of energy in the emitting gas zone and in the neighboring gas zones when the banded gas radiation model is used. If the emitting beam length is calculated separately for each gas zone (this can easily be done in combination with the Monte Carlo view factor calculation), lower values for the emissive beam length than those calculated from Eq. 56 are obtained, resulting in higher absorption coefficients for the gray gas (see Figure 1).



**Table 2. Furnace Dimensions and Operating Conditions**

Furnace		
Height	(m)	7.624
Length	(m)	7.137
Width	(m)	2.002
Thickness of refractory	(m)	0.228
Thickness of insulation	(m)	0.05
Number of side burners	—	86
Number of floor burners	—	8
Reactor coils		
Number of reactors	—	4
Number of passes	—	9
External tube diameter	(mm)	115
Internal tube diameter	(mm)	101.6
Firing conditions		
Fuel gas	(ton/h)	1.273
Excess air	(%)	21
Fuel gas composition	(mol %)	See Table 3
Total heat input	(MW)	17.6
Reactor operating conditions		
Feedstock		Naphtha
Feedstock composition		
<i>n</i> -Paraffins	(wt %)	41.0
Isoparaffins	(wt %)	38.3
Naphthenes	(wt %)	13.3
Aromatics	(wt %)	7.4
Feedstock feed rate (4 coils)	(ton/h)	9.7
Steam dilution	(kg/kg)	0.35
Coil inlet temperature	(K)	873
Coil outlet pressure	(atm)	2.02
Material properties		
Emissivities	—	See Table 1
Thermal conductivity of refractory	(W/mK)	0.267
Thermal conductivity of insulation	(W/mK)	0.093
Thermal conductivity of tube skin	(W/mK)	34.88

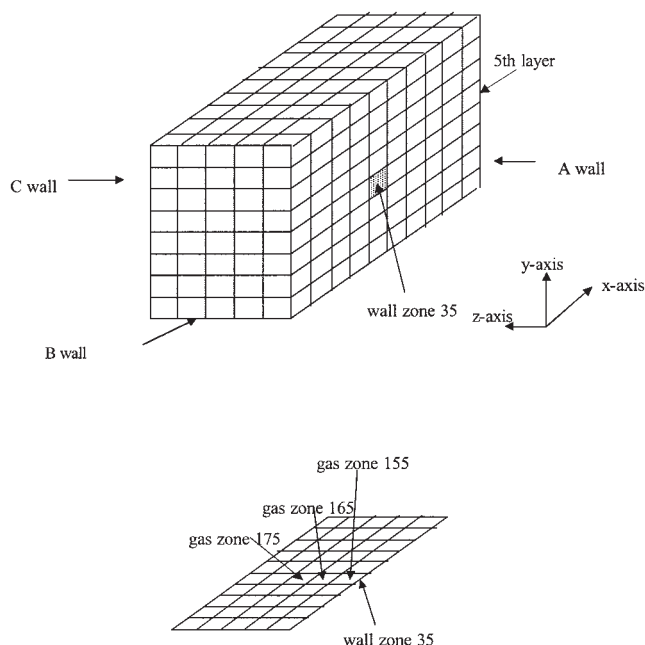
Thus, more radiation is emitted and reabsorbed by the gas zone. The absorption in the neighboring gas zones increases as well. With this correct approach of emissive beam length calculation in combination with the banded gas radiation model, good results are obtained when comparing the calculated furnace thermal efficiency to the industrial value ( $\pm 45\%$ ).

## Furnace Description

The main dimensions, operating conditions, and fuel gas composition of the simulated furnace are summarized in Tables 2 and 3, respectively. A schematic view of the simulated furnace radiation section is given in Figure 3. Four reactor coils, with nine passes each, are suspended in two staggered rows in the furnace. The furnace is heated with 86 radiation

**Table 3. Fuel Gas Composition**

Constituent		Percentage
H <sub>2</sub>	(mol%)	5.73
CH <sub>4</sub>	(mol%)	77.17
C <sub>2</sub> H <sub>4</sub>	(mol%)	0.03
C <sub>2</sub> H <sub>6</sub>	(mol%)	15.88
C <sub>3</sub> H <sub>6</sub>	(mol%)	0.04
C <sub>3</sub> H <sub>8</sub>	(mol%)	0.19
C <sub>4</sub> paraffins	(mol%)	0.89
CO	(mol%)	0.07
Total	(mol%)	100

**Figure 3. Schematic views of the furnace radiation section.**

burners, positioned in seven rows of burners in the front wall (A wall) and six rows of burners in the rear wall (C wall) of the furnace. There are eight additional floor burners. The furnace outlet is located at the top of the C wall and stretches out over the main part of the furnace length. The furnace is divided into zones by means of seven planes parallel to the furnace bottom plate, nine planes parallel to the side walls (B and D walls), and four planes parallel to the front wall. A total of 1028 isothermal zones are considered for the calculations: 288 tube wall zones, 340 furnace wall zones, and 400 gas volumes.

Seven simulations are performed. In the simulation cases 1 to 3 the effect of introducing the banded gas radiation model to replace the nonbanded gas radiation model is evaluated. In simulation case 1, the nonbanded gas radiation model is used for the gas and the gray surface radiation model for all surfaces (furnace wall and tube skin). In the simulation case 2 the nonbanded gas radiation model is replaced by the banded gas radiation model. This banded gas radiation model is then used for all following simulation cases. In simulation case 3, the furnace wall is coated but the gray surface radiation model still applies. In simulation cases 4 to 7, the effect of introducing the nongray surface radiation model is evaluated. In these four simulation cases, the effect of coating the tubes and/or the furnace walls is evaluated. In simulation case 4, the gray surface radiation model is applied, but with gray emissivities calculated from the nongray values according to

$$\sum_{z=1}^{17} \epsilon_{-z} * \text{sum } z = \epsilon_{\text{gray}} \quad (57)$$

with (see sample calculation)

**Table 4. Overview of Simulation Conditions\***

Simulation Case	Case 1		Case 2		Case 3		Case 4		Case 5		Case 6		Case 7	
Surface Model	G		G		G		G		NG		NG		NG	
Gas Model	NB	B	NB	B	NB	B	NB	B	NB	B	NB	B	NB	B
Tube														
Noncoated	+		+		+									+
Coated							+		+		+			
Furnace														
Noncoated	+		+				+		+					+
Coated					+						+			

\*G, gray; NG, nongray; B, banded gas; NB, nonbanded.

$$\sum_{z=1}^{17} \text{sum } z = 1 \quad (58)$$

The corresponding values for  $\varepsilon_{\text{gray}}$  are found in Table 1. In simulation cases 4 to 6, the tubes are coated because they act as better heat sinks. In simulation cases 5 and 6, the nongray surface radiation model is introduced. In simulation case 5, the furnace wall is uncoated. In simulation case 6, the furnace wall is coated. Finally, a simulation is performed (simulation case 7) in which both the furnace walls and the tubes are uncoated, to evaluate the maximum change in calculated thermal efficiency of a furnace resulting from complete coating. An overview of the radiation models used for the different simulations is given in Table 4.

In Table 1 the variation of the emissivity of the different solid materials is given as a function of wavelength.

## Results and Discussion

The goal of the simulations is to determine the influence of applying high-emissivity coatings on the thermal efficiency of steam-cracking furnaces. To evaluate the effects of the introduction of the banded gas radiation model, simulation cases 1 and 2 are compared in some detail. In Table 5, some calculation results for gas zone 165 are presented for simulation cases 1 and 2. As seen in Figure 3, this gas zone is situated in the fourth horizontal layer of the furnace grid. For this gas zone the precisely calculated emissive beam length is 1586 mm, as compared to the furnace averaged value of 2595 mm calculated according to Eq. 56. When using the nonbanded gas radiation model, the self-absorption of the gas is lowered by a factor of about 2.4 compared to that of the banded gas radiation model. Thus, if the thermal efficiency of the furnace is to be calculated correctly with the nonbanded gas radiation model, the total

amount of radiative energy emitted by the gas zones has to decrease accordingly. This means that a lower absorption coefficient (or a higher emissive beam length) is required with the nonbanded gas radiation model to attain the same thermal efficiency as with the banded gas radiation model. The effect of the strong self-absorption, when using the banded gas radiation model, is reflected in the radiative heat exchange between neighboring gas zones. In Table 6, calculation results for the radiative heat exchange between the two neighboring gas zones 165 and 166 are presented for simulation cases 1 and 2.

From the total exchange area values between these zones presented in Table 6, it is clear that the amount of radiative energy emitted by a gas zone and absorbed by a neighboring gas zone is also about a factor of 2.0 higher when the banded gas radiation model is used, compared to the nonbanded gas radiation model. From the radiative energy actually leaving gas zone 165, a larger part is absorbed in the neighboring gas zones. This increase is explained by a corresponding increase of the total exchange area between neighboring gas zones 165 and 166. Thus, the use of the banded gas radiation model to replace the nonbanded gas radiation model results in a stronger self-absorption (factor 2.4) by the emitting gas zone and a stronger absorption (factor 2.0) in the neighboring gas zones. This process of emission and almost immediate (re-)absorption of radiative energy should result in a more uniform temperature profile in the gas zones, except for those gas zones where this is not possible because of the presence of heat sinks (such as the reactor tubes). This is confirmed in Figure 4 where the flue gas temperature profile between the two long furnace walls A and C is presented at the level of the fifth horizontal layer of gas zones. The correctness of this conclusion is confirmed by an additional simulation (case 2\*), in which the number of gas (and furnace wall) zones in the furnace is augmented: the furnace is divided by ten instead of four planes parallel to the front wall A. The calculated flue gas temperature profile between the long furnace walls A and C for the fifth layer in

**Table 5. Radiation Properties for Gas Zone 165**

	Nonbanded Gas Model	Banded Gas Model
Simulation case	Case 1	Case 2
Emissive beam length (mm)	2595	1586
Temperature of gas zone 165 (K)	1534.3	1565.1
Total emitted energy (W)	32,553	44,594
Self-absorption (W)	2891	9331
Self-absorption to total emission (%)	8.9	20.9
Transmissivity for $k$ calculation	0.7503	0.8008
Absorption coefficient $k$ ( $\text{m}^{-1}$ )	0.1107	0.1401
Thermal efficiency of the furnace (%)	45.4	46.2

**Table 6. Radiative Heat Exchange between Gas Zones 165 and 166**

	Nonbanded Gas Model	Banded Gas Model
Simulation case	Case 1	Case 2
Input (from 166 to 165) (W)	263	725
$G_{166}G_{165}$ (from 166 to 165) ( $\text{m}^2$ )	0.000839	0.002127
Output (from 165 to 166) (W)	266	736
$G_{165}G_{166}$ (from 165 to 166) ( $\text{m}^2$ )	0.000843	0.002152
Percentage of output to total emitted energy (see Table 5) (%)	0.82	1.65

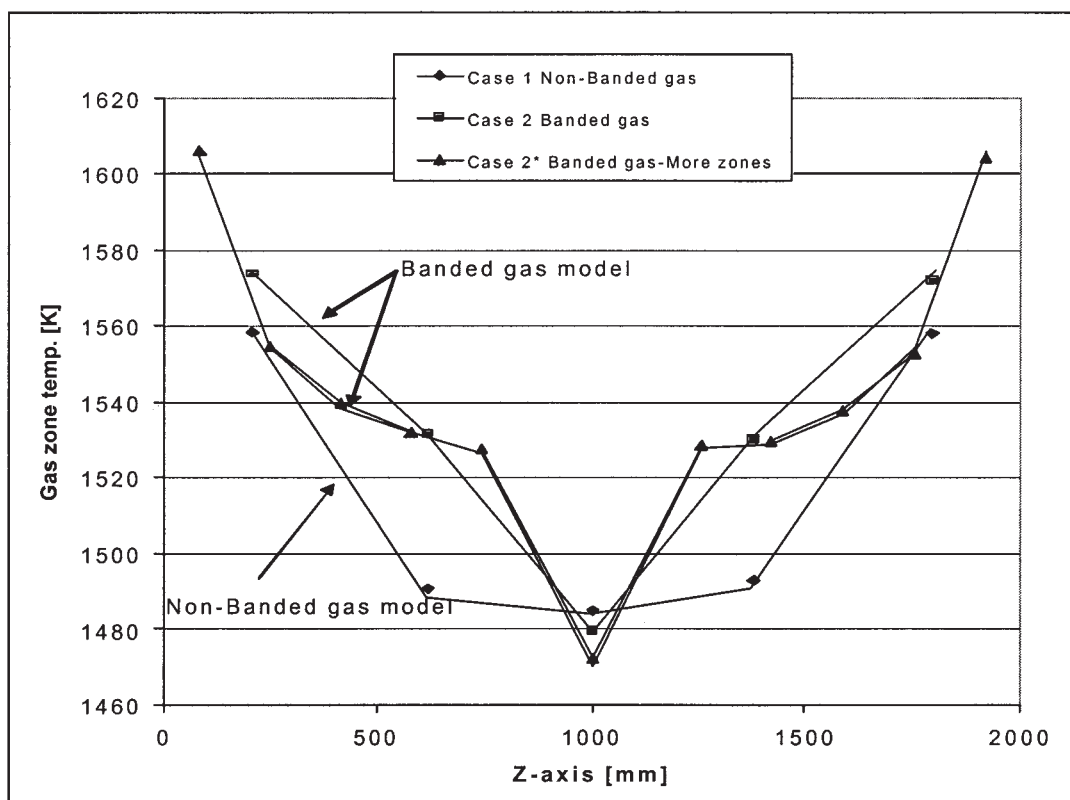


Figure 4. Flue gas temperature profiles.

5th layer in height; 3rd layer along the x-axis.

height is also presented in Figure 4 (case 2\*). The effect of a gas temperature uniformization between the long furnace walls and the row of tubes, on one hand, and the existence of a heat sink in the middle of the furnace, on the other hand, are confirmed by this simulation. This step-by-step behavior of radiative heat exchange between neighboring gas zones is analogous to the behavior of convective and conductive heat exchange.

The calculation results, an overview of which is presented in Table 7, show that, by the introduction of the banded gas radiation model, the calculated furnace thermal efficiency increases from 45.4% (case 1) to 46.2% (case 2). In other words, both the nonbanded gas radiation model (case 1) and the banded gas radiation model (case 2) are able to calculate the

correct, industrially observed thermal efficiency of the furnace, but require the use of completely different values for the emissive beam length to calculate the gas absorption coefficients. For the banded gas radiation model this emissive beam length is a gas zone-dependent, calculated value. For the nonbanded gas radiation model, an averaged value, which can be considered as a model parameter, is used. The use of the banded gas radiation model also results in the calculation of a completely different flue gas temperature profile between the front (A) and the rear (C) walls of the furnace. This difference in the shape of the flue gas temperature profile is calculated for all heights in the furnace. In the lower parts of the furnace, the flue gas temperature values calculated with the nonbanded gas radiation model are higher than those calculated with the

Table 7. Simulation Results

	Simulation Case						
	Case 1	Case 2	Case 3	Case 4	Case 5	Case 6	Case 7
Conversion (%)	98.62	99.01	98.96	98.62	96.59	97.88	92.48
COT (°C)	839.6	847.1	846.2	839.8	816.4	829.5	791.7
$T_{w,ext}^{max}$ (°C)	955.5	963.1	963.6	955.7	930.7	944.2	899.4
Yields (mass fraction)							
Ethylene	0.2556	0.2601	0.2595	0.2556	0.2386	0.2487	0.2149
Propylene	0.1430	0.1365	0.1374	0.1431	0.1605	0.1515	0.1700
Benzene	0.09531	0.1017	0.1007	0.09514	0.07681	0.08673	0.05945
1,3-Butadiene	0.04183	0.04171	0.04177	0.04190	0.04105	0.04183	0.03818
Methane	0.1797	0.1850	0.1842	0.1795	0.1610	0.1715	0.1391
Hydrogen	0.00713	0.007311	0.00728	0.00712	0.00650	0.00686	0.005745
PER	0.5595	0.5248	0.5295	0.5599	0.6727	0.6092	0.7911
$\eta_{tot}$ (%)	45.41	46.24	46.12	45.44	42.66	44.26	39.14

**Table 8. Temperatures (K) of the Selected Zones**

	Case 1 (Nonbanded Gas)	Case 2 (Banded Gas)
Tube zone 60	1175.9	1179.7
Wall zone 35	1332.5	1333.4
Gas zone 155	1592.4	1606.6
Gas zone 165	1534.3	1565.1
Gas zone 175	1554.8	1531.3

banded gas radiation model over the entire  $z$ -axis. In both the middle section and the top section of the furnace, the flue gas temperatures calculated with the nonbanded gas radiation model retain the highest values only near the long furnace walls A and C (see Figures 3 and 4). However, it is remarkable that, on average, in all three cases (1, 2, and 2\*), the flue gas temperatures in the gas zones containing the tubes (that is, the heat sinks) remain rather invariant.

In a further comparison of simulation cases 1 and 2, the heat exchanges between a tube zone, a wall zone, and the three intermediate gas zones in a horizontal layer in the furnace are evaluated. However, because the total amount of radiation exchanged between two zones depends on the temperature of the emitting zone (total amount of emitted energy) and on the temperature of the flue gas in between both zones (flue gas transmissivity), and as the temperatures of the zones calculated in the two simulation cases differ (see Table 8), it was decided to compare total exchange areas between the zones instead of total amounts of radiation, to exclude the temperature effect as much as possible. Furthermore, the observations in the previous paragraphs, with respect to the change of the total exchange areas by replacing the nonbanded gas radiation model with a banded gas radiation model, can be validated. The selected zones (on a horizontal line) are (see Figure 3):

- Tube zone 60 (located in gas zone 175)
- Wall A zone 35 (touching gas zone 155)
- Gas zones 155, 165, 175

The total exchange areas between these zones for simulation cases 1 and 2 are given in Table 9, from which it is seen that the total exchange area between two zones does not change when the emitting zone is a surface (1a, 1b, 2a, 3a, 4a, 5a, 6a,

7a). The small differences are explained by slight changes in gas transmissivity because the gas temperatures change (see Table 8). This confirms the earlier conclusion, based on theoretical developments, that the total exchange area between two zones is unaffected by replacing the nonbanded gas radiation model with a banded gas radiation model when the emitting zone is a surface zone. When the emitting zone is a gas zone (2b, 3b, 4b, 5b, 6b, 7b, 8a, 8b, 9a, 9b, 10a, 10b), the total exchange areas change. The strongest changes of the total exchange areas are calculated for the energy exchange between gas zones (8a, 8b, 9a, 9b, 10a, 10b). Increases of total exchange areas from 50 to nearly 70% are calculated. When the emitting zone is a gas zone and the receiving zone is a surface zone (2b, 3b, 4b, 5b, 6b, 7b), changes are similar but become smaller as the zones are further apart. Again, this confirms the earlier conclusion, based on theoretical developments, that the total exchange area between two zones is affected by replacing the nonbanded gas radiation model with a banded gas radiation model when the emitting zone is a gas zone. From these changes, especially for exchange between gas zones, the step-by-step radiative heat transfer in the flue gas is confirmed. Special attention is drawn to the change (+20%) in total exchange area from the gas zone 175 to the tube zone 60 (Table 9; 4b) which is located in this gas zone.

The changes of the radiative heat transfer from the considered gas zones to the considered tube zone are visualized in Figure 5. The “heat sink” character of the tube zone and the corresponding drop in the gas zone temperature (see also Figure 4), when the nonbanded gas radiation model is replaced by a banded gas radiation model, is clearly observed. In all further simulations the banded gas radiation model is used. Simulation case 3 evaluates the influence of applying a furnace wall coating on the thermal efficiency of the furnace. The gray furnace wall emissivity is augmented from 0.59 (see Table 1) to a gray value of 0.95. The calculation results are listed in Table 7. For the furnace with coated furnace walls, a thermal efficiency of 46.1% is calculated. This value was also calculated for simulation case 2 where no furnace wall coating was applied. Although the total performance of the furnace seems

**Table 9. Total Exchange Areas between Selected Zones**

Simulation Case		Case 1 Nonbanded Gas	Case 2 Banded Gas	Difference (%)
Tube zone 60 to wall zone 35	(1a)	0.007803	0.007816	0.2
Wall zone 35 to tube zone 60	(1b)	0.007973	0.007982	0.1
Tube zone 60 to gas zone 155	(2a)	0.002027	0.002022	-0.2
Gas zone 155 to tube zone 60	(2b)	0.001320	0.001321	0.1
Tube zone 60 to gas zone 165	(3a)	0.009687	0.009564	-1.3
Gas zone 165 to tube zone 60	(3b)	0.004113	0.004235	2.9
Tube zone 60 to gas zone 175	(4a)	0.027286	0.027374	0.3
Gas zone 175 to tube zone 60	(4b)	0.004408	0.005478	19.5
Wall zone 35 to gas zone 155	(5a)	0.040133	0.039989	-0.4
Gas zone 155 to wall zone 35	(5b)	0.012548	0.01326	5.4
Wall zone 35 to gas zone 165	(6a)	0.004548	0.004501	-1.0
Gas zone 165 to wall zone 35	(6b)	0.003909	0.003824	-2.2
Wall zone 35 to gas zone 175	(7a)	0.001193	0.001208	1.2
Gas zone 175 to wall zone 35	(7b)	0.001040	0.00115	9.6
Gas zone 155 to gas zone 165	(8a)	0.001136	0.002966	61.7
Gas zone 165 to gas zone 155	(8b)	0.001392	0.003145	55.7
Gas zone 155 to gas zone 175	(9a)	0.000195	0.0004	51.3
Gas zone 175 to gas zone 155	(9b)	0.000232	0.000515	55.0
Gas zone 165 to gas zone 175	(10a)	0.000796	0.001908	58.3
Gas zone 175 to gas zone 165	(10b)	0.000756	0.002265	66.6

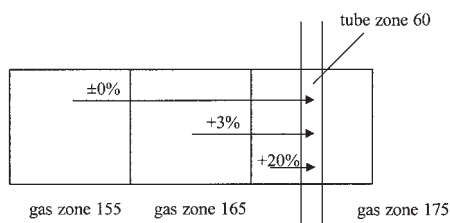


**Figure 5. Changes in total exchange area from gas zone to tube zone when the nonbanded gas radiation model is replaced by the banded radiation model.**

to be unaffected by applying a furnace wall coating, it is found that the radiative heat exchange in the furnace is substantially affected, but in a symmetrical way (not shown). The total exchange area values from a furnace wall zone to a tube zone or to a gas zone in the furnace increase by 60% when the furnace wall zone is coated. However, the total exchange area values from that same tube or gas zone to the furnace wall zone change correspondingly. It is clear that applying a banded gas radiation model, in combination with a gray surface radiation model in the furnace calculations, does not suffice to calculate the effect of furnace wall coating on furnace performance. Because of the change in furnace wall emissivity, the average furnace wall temperature changes, such as with 6 K for the fifth layer of zones on the long furnace wall A.

In an additional simulation case with gray surfaces (not mentioned in Table 4) the tubes are coated as well. This results in a somewhat higher thermal efficiency of the furnace. The higher absorptivity/emissivity of the tubes makes them perform as better heat sinks, although the effect is negligible.

Next the influence on the calculation results of using a nongray surface radiation model to replace the gray surface radiation model is evaluated in simulation cases 4 to 6. Because no information was found on the nongray emissivities of the standard Incoloy® tubes, it was decided to carry out simulation cases 4 to 6 with coated tubes. Furthermore, the gray emissivities used in these simulation cases differ from those in cases 1

to 3: gray emissivities calculated according to Eq. 57 (see Table 1) are used. A comparison of the calculation results for simulation cases 4 to 6 is found in Table 7. By comparing simulation cases 4 and 5 (conditions, see Table 4), the influence of replacing the gray surface radiation model by a nongray surface radiation model on the calculation results for an uncoated furnace is observed. The use of the nongray surface radiation model results in a 2.8% decrease of the calculated thermal efficiency of the furnace. To evaluate the changes in heat transfer between the different zones in the furnace, it was decided to compare direct and total exchange areas between some zones. The selected zones are the same as above. The direct and total exchange areas are presented in Tables 10 and 11 respectively. From Table 10 it is concluded that the direct exchange areas change substantially when the emitting zone is a surface zone (1a, 1b, 2a, 3a, 4a, 5a, 6a, 7a). The strongest effect is felt for the direct exchange area from a furnace wall to a gas zone (5a, 6a, 7a) with changes of nearly 40%.

When the emitting zone is a tube zone (1a, 2a, 3a, 4a), the effect is smaller because tubes are heat sinks in the pyrolysis furnace. This confirms the earlier conclusion (Eq. 40), based on theoretical developments, that the direct exchange area between two zones is affected by replacing the gray surface radiation model with a nongray surface radiation model when the emitting zone is a surface zone. The direct exchange areas change only slightly when the emitting zone is a gas zone (2b, 3b, 4b, 5b, 6b, 7b, 8a, 8b, 9a, 9b, 10a, 10b). These changes are attributed to slight changes in the flue gas temperature in the furnace, which affect the calculated gas zone transmissivity values. Again, this confirms the earlier conclusion (Eq. 41), based on theoretical developments, that the direct exchange area between two zones is unaffected by replacing the gray surface radiation model with a nongray surface radiation model, when the emitting zone is a gas zone. When comparing Tables 10 and 11 it is clear that some of the changes in the direct exchange area values are hampered when the total exchange area values are calculated, whereas others are fortified by the contribution of reflection on a nongray surface wall. An important conclusion, however, is the overall negative effect

**Table 10. Direct Exchange Areas between Selected Zones**

		Case 4 Gray Surface	Case 5 Nongray Surface	Difference (%)
Tube zone 60 to wall zone 35	(1a)	0.014967	0.014655	-2.1
Wall zone 35 to tube zone 60	(1b)	0.015351	0.014327	-6.7
Tube zone 60 to gas zone 155	(2a)	0.001445	0.001559	7.9
Gas zone 155 to tube zone 60	(2b)	0.001148	0.001104	-3.8
Tube zone 60 to gas zone 165	(3a)	0.010955	0.011831	8.0
Gas zone 165 to tube zone 60	(3b)	0.004685	0.004565	-2.6
Tube zone 60 to gas zone 175	(4a)	0.03156	0.034216	8.4
Gas zone 175 to tube zone 60	(4b)	0.006119	0.00606	-1.0
Wall zone 35 to gas zone 155	(5a)	0.066489	0.084564	27.2
Gas zone 155 to wall zone 35	(5b)	0.022188	0.021256	-4.2
Wall zone 35 to gas zone 165	(6a)	0.007294	0.009893	35.6
Gas zone 165 to wall zone 35	(6b)	0.006289	0.006151	-2.2
Wall zone 35 to gas zone 175	(7a)	0.001331	0.001822	36.9
Gas zone 175 to wall zone 35	(7b)	0.001726	0.001717	-0.5
Gas zone 155 to gas zone 165	(8a)	0.002747	0.002555	-7.0
Gas zone 165 to gas zone 155	(8b)	0.002731	0.00259	-5.2
Gas zone 155 to gas zone 175	(9a)	0.000297	0.000278	-6.4
Gas zone 175 to gas zone 155	(9b)	0.000378	0.000366	-3.2
Gas zone 165 to gas zone 175	(10a)	0.001695	0.001628	-4.0
Gas zone 175 to gas zone 165	(10b)	0.002123	0.00208	-2.0



**Table 11. Total Exchange Areas between Selected Zones**

		Case 4 Gray Surface	Case 5 Nongray Surface	Difference (%)
Tube zone 60 to wall zone 35	(1a)	0.004586	0.005021	9.5
Wall zone 35 to tube zone 60	(1b)	0.004702	0.004064	-13.6
Tube zone 60 to gas zone 155	(2a)	0.00213	0.0024	12.7
Gas zone 155 to tube zone 60	(2b)	0.001311	0.001239	-5.5
Tube zone 60 to gas zone 165	(3a)	0.008489	0.009316	9.7
Gas zone 165 to tube zone 60	(3b)	0.003776	0.00378	0.1
Tube zone 60 to gas zone 175	(4a)	0.024231	0.026585	9.7
Gas zone 175 to tube zone 60	(4b)	0.004842	0.004974	2.7
Wall zone 35 to gas zone 155	(5a)	0.025769	0.029034	12.7
Gas zone 155 to wall zone 35	(5b)	0.008635	0.009015	4.4
Wall zone 35 to gas zone 165	(6a)	0.002987	0.003414	14.3
Gas zone 165 to wall zone 35	(6b)	0.002535	0.002653	4.7
Wall zone 35 to gas zone 175	(7a)	0.001007	0.000987	-2.0
Gas zone 175 to wall zone 35	(7b)	0.00081	0.000844	4.2
Gas zone 155 to gas zone 165	(8a)	0.003018	0.002874	-4.8
Gas zone 165 to gas zone 155	(8b)	0.003293	0.003249	-1.3
Gas zone 155 to gas zone 175	(9a)	0.000478	0.000458	-4.2
Gas zone 175 to gas zone 155	(9b)	0.000587	0.000605	3.1
Gas zone 165 to gas zone 175	(10a)	0.00203	0.00195	-3.9
Gas zone 175 to gas zone 165	(10b)	0.002296	0.002253	-1.9

for tube zone 60 when replacing the gray surface radiation model with a nongray surface radiation model. When the tube zone is the emitting zone (1a, 2a, 3a, 4a), the total exchange area increases, whereas it mostly decreases (1b, 2b) or remains invariant (3b, 4b) when the tube zone is the absorbing zone. As a result the thermal efficiency of the furnace decreases, as seen in Table 7, when comparing the calculation results for cases 4 and 5.

It was mentioned earlier that using a gray surface radiation model, in combination with a banded gas radiation model, does not suffice to calculate a possible effect of applying a coating on the thermal efficiency of the furnace. When the changes of corresponding total exchange areas were compared when a gray surface radiation model was used for both the noncoated and the coated walls, changes up to 60% were calculated. However, these changes were symmetrical and no net effect on the furnace performance was observed: the thermal efficiency of the furnace remains unchanged. When comparing simulation cases 5 and 6, where a coating is applied on the furnace wall

and calculations are based on a nongray surface radiation model, it is clear that applying a furnace wall coating does influence the furnace thermal efficiency: an increase in furnace thermal efficiency of about 1.5% is calculated (Table 7). The nongray surface radiation model shows that the total exchange areas between the zones are influenced in an asymmetrical way when applying a furnace coating: the total exchange areas (Table 12) from the coated furnace wall zone to the tube zone (1b) increase more than the total exchange area from the tube zone to the coated furnace wall zone (1a). As a consequence, a net effect on the thermal efficiency of the furnace is calculated.

Finally, a last simulation case 7 is performed in which the tubes and the furnace walls are uncoated. The emissivity values for the tubes are those of a normal steel alloy (see Table 1). A decrease in thermal efficiency of >5%, compared to the completely coated simulation case 6, is calculated (see Table 7). An increase in thermal efficiency of about 3.5% is thus calculated when the tubes are coated in an uncoated furnace.

Typical flue gas and furnace wall temperature profiles for

**Table 12. Total Exchange Areas between Selected Zones**

		Case 5 Nongray Surface Uncoated	Case 6 Nongray Surface Coated	Difference (%)
Tube zone 60 to wall zone 35	(1a)	0.005028	0.008717	73.4
Wall zone 35 to tube zone 60	(1b)	0.004096	0.008399	105.1
Tube zone 60 to gas zone 155	(2a)	0.002413	0.001646	-31.8
Gas zone 155 to tube zone 60	(2b)	0.001183	0.000984	-16.8
Tube zone 60 to gas zone 165	(3a)	0.009317	0.009089	-2.4
Gas zone 165 to tube zone 60	(3b)	0.00363	0.003554	-2.1
Tube zone 60 to gas zone 175	(4a)	0.026612	0.026278	-1.3
Gas zone 175 to tube zone 60	(4b)	0.004824	0.004758	-1.4
Wall zone 35 to gas zone 155	(5a)	0.029472	0.052644	78.6
Gas zone 155 to wall zone 35	(5b)	0.008598	0.016225	88.7
Wall zone 35 to gas zone 165	(6a)	0.003556	0.006047	70.1
Gas zone 165 to wall zone 35	(6b)	0.0024	0.00454	89.2
Wall zone 35 to gas zone 175	(7a)	0.000994	0.002006	101.8
Gas zone 175 to wall zone 35	(7b)	0.000749	0.001379	84.1
Gas zone 155 to gas zone 165	(8a)	0.003216	0.003155	-1.9
Gas zone 165 to gas zone 155	(8b)	0.003584	0.003254	-9.2
Gas zone 155 to gas zone 175	(9a)	0.000496	0.000453	-8.7
Gas zone 175 to gas zone 155	(9b)	0.000657	0.000523	-20.4
Gas zone 165 to gas zone 175	(10a)	0.002159	0.002157	-0.1
Gas zone 175 to gas zone 165	(10b)	0.002534	0.002504	-1.2

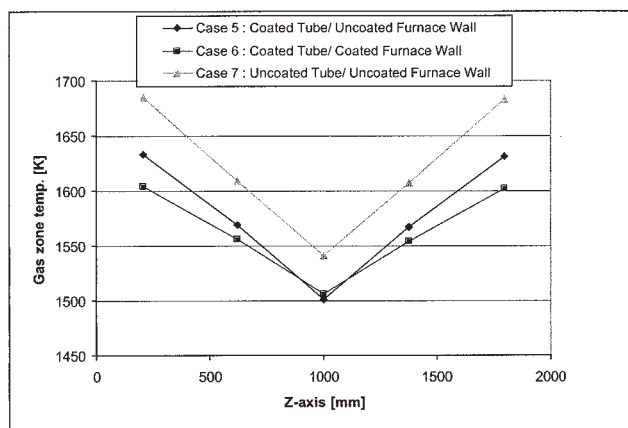


**Figure 6. Flue gas temperature profiles.**

5th horizontal layer; 3rd layer along the x-axis.

simulation cases 5 to 7, using the banded gas radiation model and the nongray surface radiation model, are shown in Figures 6 and 7. Figure 6 shows that the highest gas temperatures are calculated for case 7. This corresponds with the condition that the lowest thermal efficiency is calculated when both the furnace wall and the tube skin are uncoated. The lowest flue gas temperature profiles are calculated for case 6: the furnace walls and the tube skins are now both coated, resulting in the highest thermal efficiency. From Figure 7 it is seen that the furnace wall temperatures are highest when they are not coated (case 5). The lowest furnace wall temperatures are calculated for simulation case 6 with the coated furnace walls and the highest furnace thermal efficiency. The slight asymmetry of the furnace wall profiles is ascribed to the asymmetry of the double tube arrangement in the firebox.

Other calculated profiles for simulation cases 6 and 7 are presented in Figures 8, 9, and 10. Figure 8 compares the calculated heat flux profiles. By applying coatings, the heat fluxes increase considerably. The calculated differences are high in the bottom region of the furnace (maximum peaks where the flue gas temperatures are high). In the top of the furnace these differences are lower because the flue gas temperatures in the top of the furnace are relatively higher for the simulation cases with lower thermal efficiency. Figure 9 shows

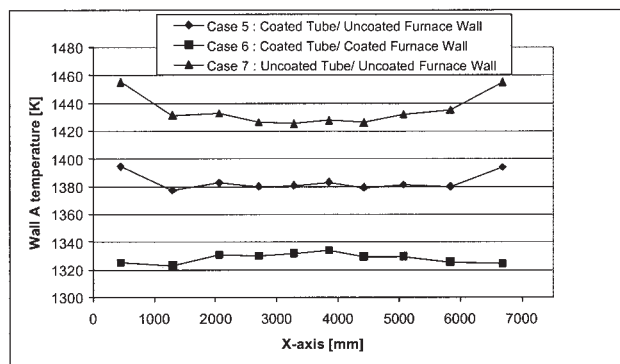


**Figure 7. Long furnace wall (A wall) temperature profiles.**

5th horizontal layer.

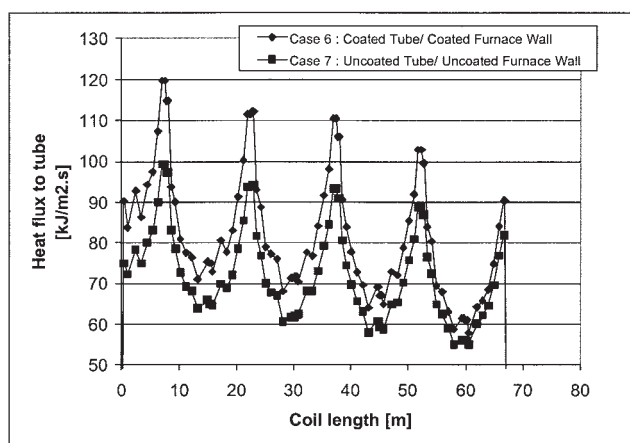


**Figure 8. Heat flux profiles along the coil.**

the corresponding external tube skin temperature profiles. At the end of the furnace coil, the difference in tube skin temperatures can be nearly 50 K (see Table 7). If the reactor and/or furnace conditions are not changed when a coating is applied to the furnace wall, the furnace run length will substantially decrease because of higher coking rates and quickly rising external tube skin temperatures. Finally, Figure 10 shows the calculated process gas temperature profiles. As seen in Table 7, the coil outlet temperature (COT) differs by nearly 40 K when the furnace walls and the tubes are coated.

The increase in the thermal efficiency of a furnace can be translated into an increase of yields, an increase of throughput, or a decrease in fuel gas input. Additional simulations can be performed to determine the optimal operating conditions.

## Conclusion

The introduction of a nongray surface radiation model, in combination with a banded gas radiation model, to calculate the radiative heat exchange in pyrolysis furnaces, allows evaluation of the effect of applying furnace wall and/or tube skin high-emissivity coatings in thermal cracking furnaces. For a naphtha cracking furnace, a 5% increase of the furnace thermal performance is calculated when furnace walls and tube skins are coated. This increase in the thermal efficiency of a furnace

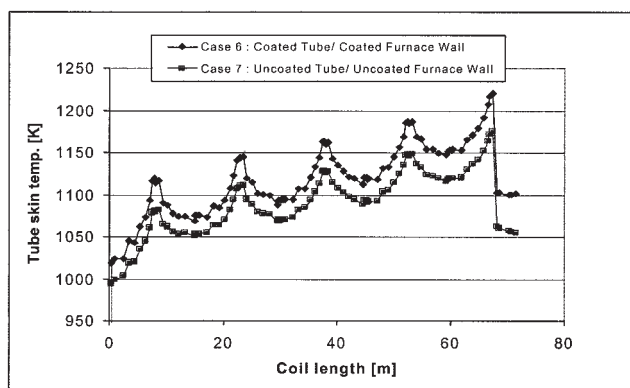


**Figure 9. External tube skin temperature profiles along the coil.**

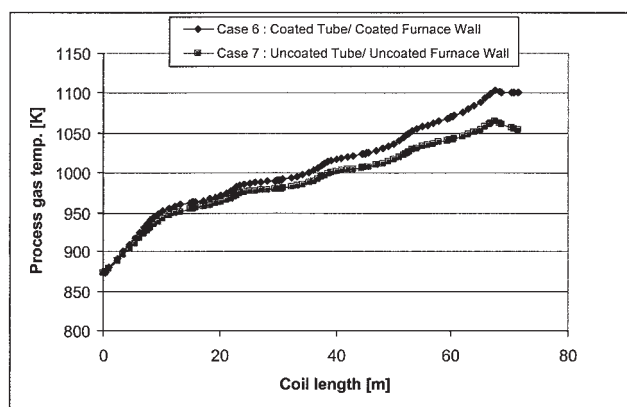


**Figure 10. Process gas temperature profiles along the coil.**

can be translated into an increase of yields, an increase of throughput, or a decrease in fuel gas input.

## Acknowledgments

G. J. Heynderickx is grateful to the Fund for Scientific Research-Flanders (FWO-N) for financial support of the CFD research in thermal cracking. The generous financial support from Asahi Kasei Co. (Japan) also made this research possible.

## Notation

$A_i$  = surface of zone  $i$ ,  $m^2$   
 COT = coil outlet temperature  
 dark  $b$  = equivalent band area calculated from the equivalent band absorption model of Edwards (see Figure 2)  
 $f_p$  = fraction  
 $F_{ij}^0$  = view factor in transparent medium  
 $g_{k,i}$  = direct exchange area between the gas volume  $k$  and the surface zone  $i$ ,  $m^2$   
 $G$  = total radiation,  $W/m^2$   
 $J$  = total emission,  $W/m^2$   
 $k$  = absorption coefficient,  $m^{-1}$   
 PER = propylene-to-ethylene ratio  
 $Q_i$  = nonradiative heat flux to zone  $i$ ,  $W/m^2$   
 $s_{i,j}$  = direct exchange area between the surface zones  $i$  and  $j$ ,  $m^2$   
 sum  $b$  = total emission area in band  $b$  (see Figure 2)  
 $S$  = distance,  $m$   
 $S^{(e)}$  = averaged emissive beam length,  $m$   
 $T$  = temperature,  $K$   
 $T_{w,ext}^{max}$  = maximum external tube wall temperature,  $^{\circ}C$   
 $V_k$  = volume of zone  $k$ ,  $m^3$   
 $W$  = emissive power,  $W/m^2$   
 $W_z$  = black body emissive power,  $W/m^2$   
 $Z_{i,j}$  = total exchange area between zones  $i$  and  $j$ ,  $m^2$

## Greek letters

$\alpha$  = absorptivity  
 $\delta_{ij}$  = Kronecker delta  
 $\varepsilon$  = emissivity  
 $\eta_{tot}$  = thermal efficiency of the furnace, %  
 $\lambda$  = wavelength,  $m$   
 $\rho$  = reflectivity  
 $\sigma$  = Boltzmann constant,  $5.67 \times 10^{-8} W m^{-2} K^{-4}$   
 $\tau$  = transmissivity

## Literature Cited

- Hellander JC. Throughput enhancement and tube temperature stabilization. *Hydrocarb Process.* 1997;76:91-96.
- Heynderickx GJ, Nozawa M. High-emissivity coatings on reactor tubes and furnace walls in steam cracking furnaces. *Chem Eng Sci.* 2004;59:5657-5662.
- Edwards DK, Glassen LK, Hauser WC, Tuschsch JS. Radiation heat transfer in nonisothermal nongray gases. *J. Heat Transfer.* 1967;89(C): 219.
- Siegel R, Howell JR. *Thermal Radiation Heat Transfer.* New York, NY: McGraw-Hill; 1972.
- Tucker RJ, Lorton R. Mathematical modeling of load-recuperative gas-fired furnaces. Proc of the First UK National Heat Transfer Conf.; 1984;1 035-1046.
- Chang SL, Rhee KT. Useful integral function and its application in thermal radiation calculations. *Commun Heat Mass Transfer.* 1983: 329-333.
- DeBellis CL. Effect of refractory emittance in industrial furnaces. Fundamentals of radiation heat transfer. *ASME HTD.* 1991;160.
- Khan YU, Lawson DA, Tucker RJ. Analysis of radiative heat transfer in ceramic-lined and ceramic coated furnaces. *J Inst Energy.* 1998;71: 22-26.
- Chang SL, Golchert B, Petrick M. Numerical analysis of CFD-coupled radiation heat transfer in a glass furnace. Proc of 34th National Heat Transfer Conf.; 2000:547-554.
- Jackson JD, Yen CC. *Ceramics in Energy Applications Conference.* London: Pergamon Press; 1994.
- Jackson JD, An P, Pena-Marco I. Measurement of the total and spectral emittance of permeable ceramic materials. *C510/132/95. IMechE.* 1995:561-565.
- Heynderickx GJ, Froment GF. A pyrolysis furnace with reactor tubes of elliptical cross section. *Ind Eng Chem Res.* 1996;35:2183-2189.
- Hottel HC, Sarofim AF. *Radiative Transfer.* New York, NY: McGraw-Hill, 1967.
- Vercammen HAJ, Froment GF. Simulation of thermal cracking furnaces. In: Weekman VW, Luss S, eds. *Chemical Reaction Engineering.* ACS Symposium 65. Washington, DC: American Chemical Society; 1978.
- Vercammen HAJ, Froment GF. An improved zone method for the simulation of radiation in industrial furnaces. *Int J Heat Mass Transfer.* 1980;23:329-337.
- Plehiens PM, Froment GF. Firebox simulation of olefin units. *Chem Eng Commun.* 1989;80:81-99.
- Rao MVR, Plehiens PM, Froment GF. The coupled simulation of heat transfer and reaction in a pyrolysis furnace. *Chem Eng Sci.* 1988;43: 1223-1229.

Manuscript received Aug. 27, 2004, and revision received Jan. 31, 2005.